HHS Public Access

Author manuscript

Clin Transl Imaging. Author manuscript; available in PMC 2018 February 01.

Published in final edited form as:

Clin Transl Imaging. 2017 February ; 5(1): 29–43. doi:10.1007/s40336-016-0214-7.

Molecular imaging and fusion targeted biopsy of the prostate

Baowei Fei[1,2,3], **Peter T. Nieh**[4], **Viraj A. Master**[4], **Yun Zhang**[1], **Adeboye O. Osunkoya**[3,4,5,6], and **David M. Schuster**[1]

[1]Department of Radiology and Imaging Sciences, Emory University School of Medicine, 1841 Clifton Road NE, Atlanta, GA 30329, USA

[2]Department of Biomedical Engineering, Emory University and Georgia Institute of Technology, Atlanta, GA 30329, USA

[3]Winship Cancer Institute of Emory University, Atlanta, GA 30329, USA

[4]Department of Urology, Emory University School of Medicine, Atlanta, GA 30322, USA

[5]Department of Pathology and Laboratory Medicine, Emory University School of Medicine, Atlanta, GA 30322, USA

[6]Department of Pathology, Veterans Affairs Medical Center, Decatur, GA 30033, USA

Abstract

Purpose—This paper provides a review on molecular imaging with positron emission tomography (PET) and magnetic resonance imaging (MRI) for prostate cancer detection and its applications in fusion targeted biopsy of the prostate.

Methods—Literature search was performed through the PubMed database using the keywords “prostate cancer”, “MRI/ultrasound fusion”, “molecular imaging”, and “targeted biopsy”. Estimates in autopsy studies indicate that 50% of men older than 50 years of age have prostate cancer. Systematic transrectal ultrasound (TRUS) guided prostate biopsy is considered the standard method for prostate cancer detection and has a significant sampling error and a low sensitivity. Molecular imaging technology and new biopsy approaches are emerging to improve the detection of prostate cancer.

Results—Molecular imaging with PET and MRI shows promising results in the early detection of prostate cancer. MRI/TRUS fusion targeted biopsy has become a new clinical standard for the diagnosis of prostate cancer. PET molecular image-directed, three-dimensional ultrasound-guided biopsy is a new technology that has great potential for improving prostate cancer detection rate and for distinguishing aggressive prostate cancer from indolent disease.

Correspondence to: Baowei Fei.

Corresponding author: Baowei Fei: bfei@emory.edu and http://www.feilab.org.

Compliance with ethical standards

Ethical statement

The study was approved by the IRB of Emory University.

Conflict of interest

The authors have participated in sponsored research involving ^{18}F-fluciclovine among other radiotracers. Emory University is eligible to receive royalties for ^{18}F-fluciclovine.

Conclusion—Molecular imaging and fusion targeted biopsy are active research areas in prostate cancer research.

Keywords

Prostate cancer; Targeted biopsy; Molecular imaging; Positron emission tomography (PET); Magnetic resonance imaging (MRI); Image segmentation; Image registration

Introduction

Estimates in autopsy studies indicate that 50% of men older than 50 years of age have prostate cancer [1, 2]. In 2015, 220,800 American men were diagnosed with prostate cancer [3]. Systematic transrectal ultrasound (TRUS) guided prostate biopsy is considered the standard method for prostate cancer detection. The current 12-core template biopsy technique has a significant sampling error and a low sensitivity (24–52%) [4–7], and it can miss up to 30% of cancers [8]. As a result, a patient may have a "negative" biopsy, but may, in fact, be harboring an occult cancer. Alternatively, a diagnosis of cancer may have been made, but the patient is under-staged, because the most aggressive histologic region of the tumor has not been sampled. Because of these limitations, patient management may not be optimized.

Because of the limitations of the current biopsy approach, it is a difficult challenge for physicians to manage patients with false negative biopsies who, in fact, harbor curable prostate cancer as indicated by biochemical measurements, such as rising prostate-specific antigen (PSA). Another important challenge facing physicians is patients diagnosed on biopsy as having premalignant lesions, i.e., multifocal high-grade prostatic intraepithelial neoplasia, and, in particular, atypical small acinar proliferation (ASAP). This biopsy result is clinically significant as there is a 40–80% chance of finding cancer on repeat biopsy if there is ASAP [9]. For ASAP patients, it is vital to re-biopsy the same area. Finally, for those patients, increasing in number, who have selected active surveillance for management of prostate cancer, it is vital to be able to reliably biopsy the same cancer foci over time to ensure that these areas are not becoming de-differentiated, a finding which would move patients to be treated with definitive local therapy. Unfortunately, the current two-dimensional (2D) ultrasound provides only an imprecise localization of the abnormal findings, and it is not possible to be certain that the same area has been sampled by the repeat biopsy. Because of the limitations and uncertainty associated with the current approach, both the patient and physician face significant challenges in making treatment decisions.

Molecular imaging and new targeted biopsy technology have been developed to improve the cancer detection rate from the current standard of care practice. Magnetic resonance imaging (MRI)/TRUS fusion targeted biopsy represents a new technique to improve cancer detection rate [10–14]. Patients who are eligible for active surveillance (AS) on their initial diagnostic biopsy often receive an MRI as well as a confirmatory biopsy [15, 16]. The suspicion level on MRI correlates with likelihood of detection of high-grade prostate cancer [10, 17–19]. TRUS saturation biopsy has also been used to monitor patients on AS, but can have

significant morbidity [20]. Positron emission tomography (PET) can detect metabolic and functional aspects of cancer. Various PET tracers have been developed for prostate cancer imaging. In this review, we will focus on MRI/TRUS fusion targeted biopsy and PET molecular imaging directed, 3D ultrasound-guided biopsy of the prostate. Literature search was performed through the PubMed database using the keywords “prostate cancer”, “MRI/ultrasound fusion”, “molecular imaging”, and “targeted biopsy”. We selected the papers published in English between January 1, 2010 and April 1, 2016.

Multiparametric MRI for the prostate

MR imaging provides excellent soft-tissue contrast and has been increasingly used for the detection of prostate tumors. As shown in Fig. 1, multiparametric MRI (mp-MRI) includes T2-weighted (T2W) MRI, diffusion-weighted imaging (DWI), dynamic contrast-enhanced imaging (DCE-MR), and MR spectroscopy (MRS). The mp-MRI has proven to be an effective technique to localize high-risk prostate cancer [21, 22]. The combined use of anatomic and functional information provided by the multiparametric approach increases the accuracy of MR imaging in detecting and staging prostate cancer [21, 22]. The European Society of Urogenital Radiology (ESUR) in 2012 established the Prostate Imaging-Reporting and Data System (PI-RADS) scoring system for multiparametric MRI of the prostate [23]. The MR PI-RADS aims to enable consistent interpretation, communication, and reporting of prostate mp-MRI findings [23, 24].

Contemporary MR imaging of the prostate combines anatomic images from high-resolution T1W and T2W sequences and functional information obtained from DWI, DCEI, and MRS. The PI-RADS Prostate MR Guidelines published in 2012 suggest the use of T2W images plus 2 functional techniques [23]. The prostate anatomy is visualized with T2W images; DWI and MRS add specificity to lesion identification, while DCE-MRI has a high sensitivity in cancer detection. In the PI-RADS™ v2, the essential components of the mp-MRI prostate examination are T2W, DWI, and DCE [25]. A combination of anatomical and functional imaging is necessary to obtain high and stable accuracy in clinical practice. Below, we focus on three MR sequences that are mostly frequently used in prostate imaging.

T2-weighted MRI

The acquisition of high-resolution T2W images of the prostate is the first step in an mp-MR imaging protocol. In T2W images, the peripheral zone of the prostate has hyperintense signal, whereas the central and transition zones have low signal, allowing the zonal anatomy of the prostate to be clearly delineated. In T2W images, prostate cancer in the peripheral zone is usually depicted as a low-signal area. However, the growth pattern and the aggressiveness of the tumor can alter its appearance. T2W MR imaging has been advocated as an accurate technique in the detection of prostate cancer in the transition zone [26, 27]. In T2W MR images, the tumor region of interest has more dark pixels than bright pixels, whereas the normal tissue has more bright pixels than dark pixels. Different features, including fractal features, textural features, and signal intensity, can be used to aid in the detection of suspicious lesions. Prostate cancers at the central gland and peripheral zone usually have significantly different textures on T2W MR images [28].

Diffusion-weighted MRI

The diffusion properties of tissue are related to the amount of interstitial free water and permeability. In general, cancer tends to have more restricted diffusion than normal tissue, because of the higher cell densities and abundance of intra- and inter-cellular membranes in cancer [29]. Diffusion-weighted MRI images can be used to detect prostate cancer from differences in the diffusion of water molecules of the normal and tumor tissues [29]. The diffusion-weighted image is usually generated with different b values which can be used to calculate the apparent diffusion coefficient (ADC), and the ADC for each pixel of the image is displayed as ADC map. Diffusion of water molecules in tumor tissue is thought to reflect tissue architecture, such as cell density and nucleus/cytoplasm ratio, and reductions in ADC values. For these reasons, ADC values have received the attention as a predictor of Gleason score in prostate cancer [30, 31]. Studies show that DWI findings may indicate tumor aggressiveness [32–34]. DWI images and ADC maps are the key component of the prostate mp-MRI exam. For example, the combination of 10th percentile ADC, average ADC, and T2-weighted skewness is promising in the differentiation of prostate cancer from normal tissue [34].

Dynamic contrast-enhanced MRI

DCE-MRI, which enables visualization of vascular permeability and perfusion, is an important tool in oncology to define tumor. DCE-MRI is sensitive to alterations in vascular permeability, extracellular space, and blood flow. The clinical application of DCE-MRI for prostate cancer is based on data showing that malignant lesions show earlier and faster enhancement and earlier contrast agent washout compared with healthy prostate tissues [35]. DCE-MRI data can be analyzed with various semiquantitative or quantitative models to extract parameters related to vascular permeability, extracellular space, blood flow, and water exchange [36]. The most commonly used quantitative approach of analyzing DCE-MRI is two-compartment pharmacokinetic (PK) models that can be used to generate pharmacokinetic parameters, such as Ktrans (transfer of gadolinium contrast from the vasculature to the tumor, representing forward vascular perfusion and permeability) and Kep (reverse transfer of contrast agent from the extracellular space back to the plasma, representing backward leakage) to quantify tumor enhancement and the contrast uptake and washout [37]. DCE-MRI usually has lower spatial resolution than other sequences, especially when DCE-MRI is performed rapidly in a short period of time.

Magnetic resonance spectroscopy (MRS)

Magnetic resonance spectroscopy (MRS) is an MR technique for characterization of chemical composition in tissue. The position of each metabolite peak in the output graph reflects the resonant frequencies or chemical shifts of its hydrogen protons, and the area of each peak reflects the relative concentration of that metabolite [123]. On MRS, the resonances for the prostate metabolites, such as citrate (Cit), creatine (Cre), and choline (Cho), occur at distinct frequencies (2.60, 3.04, and 3.20 ppm for Cit, Cre, and Cho, respectively). In vivo MRS can be used for metabolite profiling in the prostate tissue to discriminate carcinomas and healthy prostate. The healthy prostate produces a high level of citrate. In prostate cancer tissue, citrate levels decrease markedly. Prostate cancer also leads

to choline increased. The metabolite ratios, such as Cho/Cit, (Cho + Cre)/Cit are significant to discriminate between prostate cancer and benign prostatic hyperplasia. The ratio of choline to citrate (Cho/Cit) is increased in cancer. The choline plus creatine to citrate ratio ([Cho + Cre]/Cit) has widely been studied and cut-off values have been suggested for the detection of prostate cancer.

MRI/TRUS fusion targeted biopsy

As the current standard of care practice for an initial prostate biopsy has a low cancer detection rate, the development and evaluation of new biopsy technology are active research areas [7, 38–51]. It has been reported that MR/TRUS fusion biopsy detects more cancer per core than standard 12-core TRUS biopsy [38]. The use of 3D tracking and image fusion has the potential to improve current methods for diagnosis and follow-up of prostate cancer [41–44].

Pinto and co-workers reported various studies on MR/TRUS fusion targeted biopsy [38–40, 52]. In a landmark prospective cohort study of 1003 men undergoing both targeted and standard biopsy concurrently from 2007 through 2014 at the National Cancer Institute (NIH) in the United States [52], targeted vs standard biopsy and the two approaches combined were assessed for the diagnosis of intermediate- to high-risk prostate cancer. Patients were referred for elevated level of PSA or abnormal digital rectal examination results, often with prior negative biopsy results. Risk categorization was compared among targeted and standard biopsy and, when available, whole-gland pathology after prostatectomy as the “gold standard”. Patients underwent mp-MRI to identify regions of prostate cancer suspicion followed by targeted MRI/TRUS fusion biopsy and concurrent standard biopsy. The primary objective was to compare targeted and standard biopsy approaches for detection of high-risk prostate cancer (Gleason score ≥ 4 + 3); secondary end points focused on detection of low-risk prostate cancer (Gleason score 3 + 3 or low-volume 3 + 4) and the biopsy ability to predict whole-gland pathology at prostatectomy. The study results show that targeted MRI/TRUS fusion biopsy diagnosed 461 prostate cancer cases, and standard biopsy diagnosed 469 cases. There was exact agreement between targeted and standard biopsy in 690 men (69%) undergoing biopsy. Targeted biopsy diagnosed 30% more high-risk cancers vs standard biopsy (173 vs 122 cases, $P < .001$) and 17% fewer low-risk cancers (213 vs 258 cases, $P < .001$). When standard biopsy cores were combined with the targeted approach, additional 103 cases (22%) of mostly low-risk prostate cancer were diagnosed (83% low risk, 12% intermediate risk, and 5% high risk). The predictive ability of targeted biopsy for differentiating low-risk from intermediate- and high-risk disease in 170 men with whole-gland pathology after prostatectomy was greater than that of standard biopsy or the 2 approaches combined (area under the curve, 0.73, 0.59, and 0.67, respectively; $P < .05$ for all comparisons). Among men undergoing biopsy for suspected prostate cancer, targeted MR/ultrasound fusion biopsy, compared with standard extended-sextant ultrasound-guided biopsy, was associated with increased detection of high-risk prostate cancer and decreased detection of low-risk prostate cancer. Future studies will be needed to assess the ultimate clinical implications of targeted biopsy.

Marks and colleagues have also published various studies on MR/TRUS fusion biopsy [53–56] and found that when suspicious lesions were targeted by MR/TRUS fusion, the positive biopsy rate per core is higher (33%) than that (7%) of the standard, systematic biopsy [45, 53, 54, 56–60], In men with prior negative biopsy and elevated PSA, fusion targeted biopsy revealed prostate cancer in 34% [56]. Marks and colleagues used an Artemis system (Eigen, Grass Valley, CA), a commercially available robot-like device that can interface with any OEM ultrasound machine to provide 3D navigation and recording for prostate biopsies. The device has the capability to plan targets for biopsy within the prostate. It has predefined biopsy plans, like the systematic 12-core plan and custom plans, as defined by the urologist. The device also has the capability to load the previous biopsy plans for re-biopsy. In addition, together with the ProFuse software package which allows a radiologist to annotate suspicious areas on mp-MRI using advanced visualization tools, Artemis is capable of mapping suspicious areas from MRI to TRUS for biopsy using MR/TRUS fusion. During biopsy, the user is able to navigate to these areas through a visual interface that shows the real-time position of the probe in multiple views (Table 1).

Molecular imaging with PET for the prostate

Positron emission tomography (PET) can detect metabolic and functional information of cancer and various PET imaging agents are under development and validation for prostate cancer detection. The ^{68}Ga-labed small-molecule inhibitor Glu-NH-CO–NH-Lys(Ahx)-HBED-CC is a new PET tracer that has been investigated for prostate cancer detection in the Europe [61–64]. PET/CT with ^{68}Ga-Prostate-Specific Membrane Antigen (PSMA) ligand shows substantially high detection rates [63]. Other PET tracers include ^{11}C-choline [65–68], ^{18}F-fluorocholine [69–71], ^{11}C-acetate [72–75], radiolabeled minibody [76], 2-^{18}F-fluoropropionic acid (^{18}F-FPA) [77], ^{18}F 16-beta-fluoro-5-alpha-dihydrotestosterone (^{18}F-FDHT) [78], radiolabeled J591 [79–81], ^{11}C-methionine [82–84], *N*-[*N*-[(*S*)-1,3-di-carboxypropyl]carbamoyl]-4-[^{18}F]fluorobenzyl-L-cysteine (^{18}F-DCFBC) [85, 86], and etc. It has been reported that ^{18}F-DCFBC PET was able to detect more clinically significant high-grade and larger-volume tumors with higher specificity than MR imaging [87]. PET imaging with ^{11}C-choline [67, 88] has been approved by the U.S. Food and Drug Administration (FDA) for prostate cancer detection and staging. PET imaging with new molecular imaging tracers, such as anti-1-amino-3-^{18}F-fluorocyclobutane-1-carboxylic acid (^{18}F fluciclovine), has shown promising results for detecting and localizing prostate cancer in humans [89, 90]. Fluciclovine (Axumin, Blue Earth Diagnostics, UK) was originally developed at Emory University and was recently approved by the U.S. FDA for detection of recurrent prostate cancer.

Fluciclovine PET molecular imaging of prostate cancer

Fluciclovine is a synthetic L-leucine analog that has been developed for detecting and staging prostate cancer with PET [91]. In a prospective study of 93 patients, Schuster et al. reported the results of fluciclovine PET imaging in recurrent prostate cancer [92]. A total of 93 patients underwent fluciclovine PET-CT plus ^{111}In-capromab pendetide single photon emission computerized tomography–computerized tomography for suspected recurrent prostate carcinoma within 90 days. In the 91 of 93 patients with sufficient data for a

consensus on the presence or absence of prostate/bed disease fluciclovine had 90.2% sensitivity, 40.0% specificity, 73.6% accuracy, 75.3% positive predictive value, and 66.7% negative predictive value compared to ^{111}Indium-capromab pendetide with 67.2, 56.7, 63.7, 75.9, and 45.9%, respectively. In the 70 of 93 patients with a consensus on the presence or absence of extraprostatic disease, fluciclovine had 55.0% sensitivity, 96.7% specificity, 72.9% accuracy, 95.7% positive predictive value, and 61.7% negative predictive value compared to ^{111}Indium-capromab pendetide with 10.0, 86.7, 42.9, 50.0, and 41.9%, respectively. Of 77 index lesions used to prove positivity histological proof was obtained in 74 (96.1%). Fluciclovine identified 14 more positive prostate bed recurrences (55 vs 41) and 18 more patients with extraprostatic involvement (22 vs 4). Fluciclovine positron emission tomography/computerized tomography correctly up-staged 18 of 70 cases (25.7%) in which there was a consensus on the presence or absence of extraprostatic involvement.

Schuster et al. also reported the correlation of fluciclovine PET images with histologic examination of the surgically removed prostate [93]. The study was also to determine if uptake correlates to markers of tumor aggressiveness, such as Gleason score. Ten patients with prostate carcinoma pre-radical prostatectomy underwent 45 min dynamic PET-CT of the pelvis after IV injection of 347.8 ± 81.4 MBq fluciclovine. Each prostate was co-registered to a separately acquired MR, divided into 12 sextants, and analyzed visually for abnormal focal uptake. Highest combined sensitivity and specificity were 81.3 and 50.0%, respectively. SUVmax was significantly higher ($P < .05$) for malignant sextants compared with non-malignant sextants, though there was overlap of activity between malignant and non-malignant sextants. SUVmax also significantly correlated ($P < .05$) with Gleason score. It is concluded that while not possessing sufficient specificity for planning of radiation therapy to the prostate, fluciclovine PET may be useful to guide biopsy to the most aggressive lesion.

Imaging with fluciclovine succeeded in identifying both primary and metastatic prostate carcinoma on the initial staging as well as uptake in recurrent prostate carcinoma within the prostate bed, lymph nodes, and bone [89]. In a study by Turkbey and colleagues [94], fluciclovine PET/CT shows higher uptake in intraprostatic tumor foci than in normal prostate tissue; however, fluciclovine uptake in tumors is similar to that in benign prostatic hyperplasia (BPH) nodules. Combined fluciclovine PET/CT and T2-weighted MR imaging enable more accurate localization of prostate cancer lesions than either modality alone [94]. PET/CT with fluciclovine shows focal uptake at the tumor and thus can provide location information to direct targeted biopsy of the prostate [93]. By combining PET/CT with 3D ultrasound images, multimodality image-guided targeted biopsy has become a promising technology for improved detection and diagnosis of prostate cancer [95].

PSMA ligand PET imaging of prostate cancer

Prostate-specific membrane antigen (PSMA) is a type II integral membrane glycoprotein, which is considered to be a well-established target antigen in prostate cancer, because it is highly and specifically expressed on the surface of prostate tumor cells at all tumor stages. In recent years, there has been increasing focus on PSMA as a target for both imaging and

therapy. Small-molecule high-affinity PSMA antagonists have been developed and are labeled with ^{68}Ga, ^{18}F, ^{11}C, ^{64}Cu, and ^{86}Y [124].

^{68}Ga-PSMA-HBED-CC PSMA (^{68}Ga PSMA) ligand is a related small-molecule PSMA antagonist that has up to now been the most clinically used PSMA PET radiotracer in prostate cancer patients. Afshar-Oromeih et al. [125] performed a retrospective analysis in 319 prostate cancer patients who underwent ^{68}Ga PSMA ligand PET/CT. The study included primary, biochemical recurrence, and metastatic cancers. ^{68}Ga PSMA can detect prostate cancer in a high percentage of patients with suspected cancer (82.8%). Tumor-detection was correlated with PSA level and androgen deprivation therapy (ADT). Lesion-based analysis demonstrated a sensitivity of 76.6%, specificity of 100%, negative predictive value of 91.4%, and positive predictive value of 100%. Eiber et al. [63] retrospectively studied 248 patients with biochemical recurrence after radical prostatectomy using ^{68}Ga PSMA and detected a malignant lesion in 89.5%. Detection rates improved with higher PSA levels and higher PSA velocity. The high sensitivity and excellent specificity of ^{68}Ga-PSMA were also reported by other studies [126, 127].

PSMA ligands may also be labeled with ^{18}F for PSMA PET imaging. Pomper et al. [128] reported the study of PET with small-molecule inhibitors of PSMA for the imaging of prostate cancer in animals using *N*-[*N*-[(*S*)-1,3-dicarboxypropyl]carbamoyl]-*S*-[^{11}C]methyl-L-cysteine, a glutamate-urea-cysteine (^{18}F-DCFBC) analog. A human study reported by Cho et al. [129] demonstrated the feasibility and potential of using ^{18}F-DCFBC for the detection of metastatic prostate cancer. In evaluating localized prostate cancer, Rowe et al. [87] studied 13 patients scheduled for prostatectomy who were imaged with ^{18}F-DCFBC PET, with 12 of 13 patients also undergoing prostate MR imaging. ^{18}F-DCFBC PET was able to detect more clinically significant high-grade and larger-volume tumors (Gleason score 8 and 9) with higher specificity than MR imaging.

PET/ultrasound fusion targeted biopsy

Fei and colleagues developed an approach for PET molecular image-directed, 3D ultrasound-guided biopsy [96, 97]. As shown in Fig. 2, the system uses: (1) passive mechanical components for guiding, tracking, and stabilizing the position of a commercially available transrectal ultrasound probe; (2) software components for acquiring and reconstructing a series of real-time 2D TRUS image slices into a 3D image volume of the prostate; and (3) software that segments the prostate gland in the 3D TRUS image volume and then displays a 3D model to guide a biopsy needle to the suspicious target lesions in three dimensions. The system allows real-time tracking and recording of the 3D position of the biopsy sites as a physician manipulates the ultrasound transducer. An offline workstation system is used to register and fuse PET/CT and ultrasound images.

Clinical workflow

The clinical protocol for PET/CT directed, 3D ultrasound-guided biopsy of the prostate is shown in Fig. 3. Before undergoing the targeted biopsy, the patient undergoes a PET/CT scan as part of his examination. The anatomic CT images are registered with the PET images for improved localization of the prostate and suspicious lesions. (1) The patient undergoes a

3D ultrasound scan ("pre-biopsy" image) before the actual biopsy appointment. This planning scan may be performed at any time before the biopsy and even on the same day of the PET/CT scan. (2) The PET/CT and pre-biopsy ultrasound images are registered offline before biopsy. (3) Immediately before biopsy, another 3D ultrasound image volume is acquired before the biopsy planning. These "intra-biopsy" ultrasound images are registered with the pre-biopsy ultrasound image volume. As the pre-biopsy ultrasound image volume has been registered with the PET/CT volumes; in turn, the PET/CT image is also registered with the intra-biopsy ultrasound image volume for tumor targeting. Three-dimensional visualization tools are then used to guide the biopsy needle to a suspicious lesion. (4) The position of the needle tip is recorded on real-time ultrasound images during the biopsy procedure. The location information of biopsy cores is saved and can be restored in a re-biopsy procedure if necessary. This allows the physician to re-biopsy the same area and monitor potential progression or treatment effect of a lesion. The location information of the biopsy cores can also be used to guide another additional biopsy to different locations if the original biopsy was negative. Figure 4 shows the clinical setup of the PET molecular image-directed, 3D ultrasound-guided biopsy.

Prostate segmentation and deformable registration

To use the 3D model of the prostate to guide a biopsy needle to the targeted, two key techniques are required for fusion targeted biopsy. The first technique is automatic segmentation of the prostate on the 3D TRUS image volume. The second technique is deformable registration between the 3D TRUS image volume and molecular images (PET/CT or mp-MRI).

Image segmentation

Segmentation of the prostate in a 3D ultrasound volume is a key technique of the 3D ultrasound image-guided biopsy. However, segmentation of the prostate in ultrasound images can be challenging because of shadowing from the bladder and because of low contrast between the prostate and adjacent tissue. Fei et al. developed an automatic method to segment the prostate in 3D TRUS images [97, 98]. This method utilizes the wavelet-based texture extraction technique followed by support vector machines (SVMs) to adaptively collect texture priors of prostates and non-prostate tissues and classify tissues in different sub-regions around the prostate boundary by statistically analyzing their textures using wavelet features [98]. Figure 5 shows the 3D prostate after image segmentation.

Extensive work has been carried out to develop methods to successfully segment the prostate from MR images [99–106]. It can also be challenging to accurately segment the prostate in T2W-MRI. Contour- and shape-based methods [107–111] exploit edge information and shape features to segment the prostate. One group of methods involves edge-based segmentation. The edge detection operators are used to produce edges on MR images. The candidate edges are picked up and then connected to obtain the prostate boundary. Zwiggelaar et al. [107] developed a semi-automatic method to segment the prostate in MRI data. The edge detection and non-maximum suppression are used to track the boundary of the prostate. The second group of methods involves deformable model based segmentation.

Kass et al. [112] proposed an active contour model and used image gradient to evolve a curve for segmentation. Chan and Vese [113] proposed a level set algorithm of the piecewise constant variant of the Mumford-Shah model [114] for segmentation.

Other segmentation methods have also proposed for prostate. Ghose et al. [115] reviewed segmentation methods for the prostate in TRUS, MR and CT images. Klein et al. [116] proposed an atlas-based method for segmenting the prostate in 3D MR images. Egger [117] studied a graph-based approach to automatically segment prostate based on a spherical template. Mahapatra and Buhmann [100] suggest a fully automatic method for prostate segmentation using random forests classifiers and graph cuts. Finally, Tian et al. advocate a supervoxel-based segmentation method for the prostate [118, 119].

Image registration

Image registration is a process of aligning two or more images, which aims to find the optimal transformation that best aligns the structures of interest in the input images. For molecular image directed, 3D ultrasound-guided biopsy, registration incorporates the data obtained from high sensitivity molecular imaging with real-time ultrasound for targeted biopsy of suspicious lesions.

To incorporate lesion information from PET/CT into the 3D ultrasound-guided biopsy, image registration plays a key role in combining the two imaging multimodalities. However, deformable registration of ultrasound and PET/CT images is difficult for the following reasons: (1) neither PET nor ultrasound contains enough structural information about the prostate for direct intensity-based image registration; (2) ultrasound provides only a small field of view that covers just the prostate and surrounding tissue which is only a small portion of a PET image that includes the entire pelvic region; and (3) the significant prostate deformation caused by the transrectal probe disqualifies registration algorithms that assume small deformation. Fei et al. [120, 121] used CT images as the bridge to register PET with TRUS, because both PET and CT images are acquired from a combined PET/CT system. The registration method is a hybrid approach that simultaneously optimizes the similarities from point-based registration and volume matching methods. The 3D registration is obtained by minimizing the distances of corresponding points at the surface and within the prostate and by maximizing the overlap ratio of the bladder neck on both images. The hybrid approach not only capture deformation at the prostate surface and internal landmarks but also the deformation of the entire organ.

For MRI/TRUS fusion targeted biopsy, image registration is needed to integrate the features from different images of mp-MRI, such as DCE-MRI and T2W MRI. The registration of images requires the selection of the feature space, a similarity measure, a transformation type, and a search strategy [122]. The DICOM header of MR images can provide coordination and orientation information that are useful for registering T2W, ADC, and K^{trans} maps. T2W-MRI is considered as the reference. Other modalities can be registered to T2W-MRI by aligning the coordinates of their origins, which are obtained from the DICOM header. If necessary, resolution adjustment is also performed after the alignment.

Conclusion and future directions

Molecular image-directed, 3D ultrasound-guided biopsy represents a new trend for the diagnosis of prostate cancer and for monitoring of prostate cancer for patients on active surveillance. MRI/TRUS fusion targeted biopsy is a new standard of care, approved by U.S. Food and Drug Administration. PET/ultrasound fusion targeted biopsy is a new direction that can have an immediate impact on future patient care. (1) For patients who select active surveillance and whose biopsy result shows a low-grade, non-clinically significant tumor, an accurate biopsy can help to reduce their anxiety that often increases due to possible sampling error and the uncertainty associated with the current biopsy technique. As a false negative result may delay treatment, an accurate biopsy is extremely important for those active surveillance patients and for those patients undergone focal therapy for a small volume prostate cancer. (2) For patients diagnosed on biopsy as having premalignant lesions, i.e, high-grade prostatic intraepithelial neoplasia, and, in particular, atypical small acinar proliferation (ASAP), the biopsy result is clinically significant as there is a 40–80% chance of finding cancer on repeat biopsy if there is ASAP [9]. As there might be coexisting cancer, especially with ASAP, where the pathologist finds only a small amount of histological “atypia” that is suboptimal for a definitive diagnosis of cancer; such patients require a repeat biopsy soon after the first one. For ASAP patients, it is vital to re-biopsy the same area. Unfortunately, 2D ultrasound provides imprecise location of the abnormal findings, and it is not possible to be certain that the same area has been sampled by the repeat biopsy. 3D ultrasound image-guided biopsy is able to record the 3D location of the biopsy sites for follow-up examinations and thus will change the management of these ASAP patients. (3) If the targeted biopsy improves cancer detection rate, many patients would not need repeated biopsies, and the total number of prostate biopsies could be reduced. Furthermore, it will also reduce the potential morbidities of life-threatening sepsis and transrectal bleeding, both of which are associated with biopsy procedures. The use of PET/ultrasound fusion targeted biopsies within the diagnostic pathway may result in an enhanced detection of clinically significant disease, fewer men diagnosed with clinically insignificant disease, fewer men biopsied overall, and fewer needle deployments; thus it could transform prostate cancer management and change clinical practice from “blind” to “targeted” biopsy. (4) With the advancement of combined PET/MRI, MRI can also be directly used to guide biopsies; however, this approach can have high cost and long procedure time [7, 46–49]. (5) There are still technical challenges for molecular image-directed, 3D ultrasound-guided biopsy, which include the development of accurate, automatic, and fast segmentation methods and reliable, deformable registration algorithms. (6) The collaboration between academic medical center and industry can play an essential role in bringing new fusion targeted biopsy technology to benefit patients and change the routine clinical practice.

Acknowledgments

This work was partially supported by NIH Grants CA156775 and CA176684.

References

1. Franks LM. Proceedings: etiology, epidemiology, and pathology of prostatic cancer. Cancer. 1973; 32(5):1092–1095. [PubMed: 4757906]

2. Holund B. Latent prostatic cancer in a consecutive autopsy series. Scand J Urol Nephrol. 1980; 14(1):29–35. [PubMed: 6154966]

3. Siegel RL, Miller KD, Jemal A. Cancer statistics, 2015. CA Cancer J Clin. 2015; 65(1):5–29. [PubMed: 25559415]

4. Roehrborn CG, Andriole GL, Wilson TH, Castro R, Rittmaster RS. Effect of dutasteride on prostate biopsy rates and the diagnosis of prostate cancer in men with lower urinary tract symptoms and enlarged prostates in the combination of avodart and tamsulosin trial. Eur Urol. 2011; 59(2):244–249. [PubMed: 21093145]

5. de la Rosette J, Wink MH, Mamoulakis C, Wondergem N, ten Kate FJC, Zwinderman K, de Reijke TM, Wijkstra H. Optimizing prostate cancer detection: 8 versus 12-core biopsy protocol. J Urol. 2009; 182(4):1329–1335. [PubMed: 19683269]

6. Presti JC, O'Dowd GJ, Miller MC, Mattu R, Veltri RW. Extended peripheral zone biopsy schemes increase cancer detection rates and minimize variance in prostate specific antigen and age related cancer rates: results of a community multi-practice study. J Urol. 2003; 169(1):125–129. [PubMed: 12478119]

7. Pondman KM, Futterer JJ, ten Haken B, Kool LJS, Witjes JA, Hambrock T, Macura KJ, Barentsz JO. MR-guided biopsy of the prostate: an overview of techniques and a systematic review. Eur Urol. 2008; 54(3):517–527. [PubMed: 18571309]

8. Hricak H. MR imaging and MR spectroscopic imaging in the pre-treatment evaluation of prostate cancer. Br J Radiol. 2005; 78(2):S103–S111. [PubMed: 16306632]

9. Iczkowski KA, Bassler TJ, Schwob VS, Bassler IC, Kunnel BS, Orozco RE, Bostwick DG. Diagnosis of "suspicious for malignancy" in prostate biopsies: predictive value for cancer. Urology. 1998; 51(5):749–757. [PubMed: 9610588]

10. Meng, X., Rosenkrantz, AB., Fenstermaker, M., Mendhiratta, N., Huang, R., Deng, F., Zhou, M., Huang, WC., Lepor, H., Taneja, SS. The relationship of increasing MRI suspicion score and the identification of high grade prostate cancer on MRI fusion targeted biopsy. 2015 American Urological Association (AUA) Meeting; May 15–19, 2015; New Orleans, LA. 2015.

11. Meng, M., Rosenkrantz, AB., Mendhiratta, N., Fenstermaker, M., Huang, R., Wysock, J., Deng, FM., Melamed, J., Zhou, M., Huang, WC., Lepor, H., Taneja, SS. Outcomes of MRI-US fusion targeted biopsy in the risk stratification of active surveillance candidates. 2015 American Urological Association (AUA) Meeting; May 15–19, 2015; New Orleans, LA. 2015.

12. Kardos, SV., Pan, S., Nawaf, CB., Fan, R., Cornfeld, D., Weinreb, J., Schulam, PG., Sprenkle, PC. MRI-Fusion Prostate biopsy in first-time biopsy cohort yields increased detection of clinically significant prostate cancer using a simplified MRI grading scale. 2015 American Urological Association (AUA) Meeting; May 15–19, 2015; New Orleans, LA. 2015.

13. Jackson, M., Haddock, P., Staff, I., Dorin, R., Kesler, S., O'Loughlin, M., Meraney, A., Wagner, J. Comparative assessment of gleason scoring of prostate biopsies obtained by standard TRUS and MRI-TRUS at follow up in active surveillance patients. 2015 American Urological Association (AUA) Meeting; May 15–19, 2015; New Orleans, LA. 2015.

14. Frye, TP., Shakir, N., Abboud, S., George, AK., Merino, M., Choyke, P., Turkbey, B., Wood, B., Pinto, PA. MRI-TRUS guided fusion biopsy to detect progression on active surveillance for low and intermediate risk prostate cancer. 2015 American Urological Association (AUA) Meeting; May 15–19, 2015; New Orleans, LA. 2015.

15. Macleod, LC., Ellis, WJ., Newcomb, LF., Zheng, Y., Brooks, JD., Carroll, PR., Gleave, ME., Lance, RS., Nelson, PS., Thompson, IM., Wagner, AA., Wei, JT., Yang, HY., Lin, DW. Timing of the confirmatory biopsy in prostate cancer active surveillance: analysis of the canary prostate cancer active surveillance study (PASS). 2015 American Urological Association (AUA) Meeting; May 15–19, 2015; New Orleans, LA. 2015.

16. Satasivam, P., Poon, BY., Vargas, HA., Vickers, A., Eastham, A. Can confirmatory biopsy be skipped for active surveillance patients with negative MRI findings and a low number of positive cores on diagnostic biopsy?. 2015 American Urological Association (AUA) Meeting; May 15–19, 2015; New Orleans, LA. 2015.

17. Salami, S., Sonstegard, AM., Yaskiv, O., Turkbey, B., Villani, R., Ben-Levi, E., Rastinehad, A. Utility of multiparametric magnetic resonance imaging (mpMRI) in the evaluation of men for

active surveillance of prostate cancer. 2015 American Urological Association (AUA) Meeting; May 15–19, 2015; New Orleans, LA. 2015.

18. Algohary, A., Viswanath, S., Prasanna, P., Pahwa, S., Gulani, V., Moses, D., Shnier, R., Böhm, M., Haynes, AM., Brenner, P., Delprado, W., Thompson, J., Pulbrock, M., Stricker, P., Ponsky, L., Madabhushi, A. Quantitative assessment of T2-weighted MRI to better identify patients with prostate cancer in a screening population. 2015 American Urological Association (AUA) Meeting; May 15–19, 2015; New Orleans, LA. 2015.
19. Recabal, P., Assel, M., Lee, D., Akin, O., Coleman, J., Tong, A., Lee, J., Eastham, J., Salas, E., Scardino, P., Vargas, A., Ehdaie, B. Accuracy of MRI-targeted biopsy to reclassify Gleason grade in men on active surveillance. 2015 American Urological Association (AUA) Meeting; May 15–19, 2015; New Orleans, LA. 2015.
20. Reichard, CA., Haywood, SC., Purysko, A., Jones, JS., Klein, EA., Stephenson, A. MR-US fusion biopsy vs. TRUS saturation prostate biopsy in active surveillance. 2015 American Urological Association (AUA) Meeting; May 15–19, 2015; New Orleans, LA. 2015.
21. Puech P, Rouviere O, Renard-Penna R, Villers A, Devos P, Colombel M, Bitker MO, Leroy X, Mege-Lechevallier F, Comperat E, Ouzzane A, Lemaitre L. Prostate cancer diagnosis: multiparametric MR-targeted biopsy with cognitive and transrectal US-MR fusion guidance versus systematic biopsy—prospective multicenter study. Radiology. 2013; 268(2):461–469. [PubMed: 23579051]
22. Lawrence EM, Tang SY, Barrett T, Koo B, Goldman DA, Warren AY, Axell RG, Doble A, Gallagher FA, Gnanapragasam VJ, Kastner C, Sala E. Prostate cancer: performance characteristics of combined T(2)W and DW-MRI scoring in the setting of template transperineal re-biopsy using MR-TRUS fusion. Eur Radiol. 2014; 24(7):1497–1505. [PubMed: 24744197]
23. Barentsz JO, Richenberg J, Clements R, Choyke P, Verma S, Villeirs G, Rouviere O, Logager V, Futterer JJ. ESUR prostate MR guidelines 2012. Eur Radiol. 2012; 22(4):746–757. [PubMed: 22322308]
24. Dickinson L, Ahmed HU, Allen C, Barentsz JO, Carey B, Futterer JJ, Heijmink SW, Hoskin PJ, Kirkham A, Padhani AR, Persad R, Puech P, Punwani S, Sohaib AS, Tombal B, Villers A, van der Meulen J, Emberton M. Magnetic resonance imaging for the detection, localisation, and characterisation of prostate cancer: recommendations from a European consensus meeting. Eur Urol. 2011; 59(4):477–494. [PubMed: 21195536]
25. Weinreb JC, Barentsz JO, Choyke PL, Cornud F, Haider MA, Macura KJ, Margolis D, Schnall MD, Shtern F, Tempany CM, Thoeny HC, Verma S. PI-RADS prostate imaging—reporting and data system: 2015, version 2. Eur Urol. 2016; 69(1):16–40. [PubMed: 26427566]
26. Akin O, Sala E, Moskowitz CS, Kuroiwa K, Ishill NM, Pucar D, Scardino PT, Hricak H. Transition zone prostate cancers: features, detection, localization, and staging at endorectal MR imaging. Radiology. 2006; 239(3):784–792. [PubMed: 16569788]
27. Li H, Sugimura K, Kaji Y, Kitamura Y, Fujii M, Hara I, Tachibana M. Conventional MRI capabilities in the diagnosis of prostate cancer in the transition zone. AJR Am J Roentgenol. 2006; 186(3):729–742. [PubMed: 16498100]
28. Viswanath SE, Bloch NB, Chappelow JC, Toth R, Rofsky NM, Genega EM, Lenkinski RE, Madabhushi A. Central gland and peripheral zone prostate tumors have significantly different quantitative imaging signatures on 3 Tesla endorectal, in vivo T2-weighted MR imagery. J Magn Reson Imaging. 2012; 36(1):213–224. [PubMed: 22337003]
29. Joseph H, Yacoub M, Aytekin Oto, Miller Frank H. MR imaging of the prostate. Radiol Clin N Am. 2014; 52:811–837. [PubMed: 24889173]
30. Toivonen J, Merisaari H, Pesola M, Taimen P, Bostrom PJ, Pahikkala T, Aronen HJ, Jambor I. Mathematical models for diffusion-weighted imaging of prostate cancer using b values up to 2000 s/mm^2: correlation with Gleason score and repeatability of region of interest analysis. Magn Reson Med Off J Soc Magn Reson Med Soc Magn Reson Med. 2015; 74(4):1116–1124.
31. Boesen L, Chabanova E, Logager V, Balslev I, Thomsen HS. Apparent diffusion coefficient ratio correlates significantly with prostate cancer gleason score at final pathology. J Magn Reson Imaging JMRI. 2015; 42(2):446–453. [PubMed: 25408104]
32. Mazaheri Y, Shukla-Dave A, Hricak H, Fine SW, Zhang J, Inurrigarro G, Moskowitz CS, Ishill NM, Reuter VE, Touijer K, Zakian KL, Koutcher JA. Prostate cancer: identification with

combined diffusion-weighted MR imaging and 3D 1H MR spectroscopic imaging—correlation with pathologic findings. Radiology. 2008; 246(2):480–488. [PubMed: 18227542]

33. Peng Y, Jiang Y, Antic T, Giger ML, Eggener SE, Oto A. Validation of quantitative analysis of multiparametric prostate MR images for prostate cancer detection and aggressiveness assessment: a cross-imager study. Radiology. 2014; 271(2):461–471. [PubMed: 24533870]
34. Peng Y, Jiang Y, Yang C, Brown JB, Antic T, Sethi I, Schmid-Tannwald C, Giger ML, Eggener SE, Oto A. Quantitative analysis of multiparametric prostate MR images: differentiation between prostate cancer and normal tissue and correlation with Gleason score—a computer-aided diagnosis development study. Radiology. 2013; 267(3):787–796. [PubMed: 23392430]
35. Durmus T, Baur A, Hamm B. Multiparametric magnetic resonance imaging in the detection of prostate cancer. Aktuelle Urologie. 2014; 45(2):119–126. [PubMed: 24700068]
36. Ewing JR, Bagher-Ebadian H. Model selection in measures of vascular parameters using dynamic contrast-enhanced MRI: experimental and clinical applications. NMR Biomed. 2013; 26(8):1028–1041. [PubMed: 23881857]
37. Tofts PS, Brix G, Buckley DL, Evelhoch JL, Henderson E, Knopp MV, Larsson HB, Lee TY, Mayr NA, Parker GJ, Port RE, Taylor J, Weisskoff RM. Estimating kinetic parameters from dynamic contrast-enhanced T(1)-weighted MRI of a diffusable tracer: standardized quantities and symbols. J Magn Reson Imaging. 1999; 10(3):223–232. [PubMed: 10508281]
38. Pinto PA, Chung PH, Rastinehad AR, Baccala AA Jr, Kruecker J, Benjamin CJ, Xu S, Yan P, Kadoury S, Chua C, Locklin JK, Turkbey B, Shih JH, Gates SP, Buckner C, Bratslavsky G, Linehan WM, Glossop ND, Choyke PL, Wood BJ. Magnetic resonance imaging/ultrasound fusion guided prostate biopsy improves cancer detection following transrectal ultrasound biopsy and correlates with multiparametric magnetic resonance imaging. J Urol. 2011; 186(4):1281–1285. [PubMed: 21849184]
39. Rastinehad AR, Chokshi S, Benjamin CJ, Turkbey B, Chung PH, Krueker J, Xu S, Locklin JK, Gates SP, Linehan WM, Choyke PL, Wood BJ, Pinto PA. Prostate cancer detection rates using a mr/trus fusion system: in patients with a previous negative prostate biopsy. J Endourol. 2011; 25:A190.
40. Vourganti S, Rastinehad A, Yerram NK, Nix J, Volkin D, Hoang A, Turkbey B, Gupta GN, Kruecker J, Linehan WM, Choyke PL, Wood BJ, Pinto PA. Multiparametric magnetic resonance imaging and ultrasound fusion biopsy detect prostate cancer in patients with prior negative transrectal ultrasound biopsies. J Urol. 2012; 188(6):2152–2157. [PubMed: 23083875]
41. Sonn GA, Natarajan S, Margolis D, Macairan M, Lieu P, Huang J, Dorey FJ, Marks LS. Value of targeted biopsy in detecting prostate cancer using an office-based MR-US fusion device. J Urol. 2012; 187(4):E829.
42. Ukimura O, Leslie S, Lewandowski PM, Abreu ALD, Huang EYH, Shoji S, Goh A, Gross M, Agus D, Aron M, Desai M, Gill I. Impact of “image-guided targeted biopsy” on the follow-up surveillance prostate biopsy to determine progression among men on active surveillance. J Urol. 2012; 187(4):E144.
43. Banek S, Kramer U, Alloussi S, Kaufmann S, Schwentner C, Stenzl A, Schilling D. Fusion of non-contrast-3 tesla-MRI and TRUS-imaging: implementation of a new biopsy technique to detect prostate cancer. J Urol. 2012; 187(4):E591.
44. Leslie S, Goh A, Lewandowski PM, Huang EYH, Abreu ALD, Berger AK, Ahmadi H, Jayaratna I, Shoji S, Gill IS, Ukimura O. Contemporary image-guided targeted prostate biopsy better characterizes cancer volume, gleason grade and its 3d location compared to systematic biopsy. J Urol. 2012; 187(4):E827.
45. Natarajan S, Marks LS, Margolis DJ, Huang J, Macairan ML, Lieu P, Fenster A. Clinical application of a 3D ultrasound-guided prostate biopsy system. Urol Oncol. 2011; 29(3):334–342. [PubMed: 21555104]
46. Hadaschik BA, Kuru TH, Tulea C, Rieker P, Popeneciu IV, Simpfendorfer T, Huber J, Zogal P, Teber D, Pahernik S, Roethke M, Zamecnik P, Roth W, Sakas G, Schlemmer HP, Hohenfellner M. A novel stereotactic prostate biopsy system integrating pre-interventional magnetic resonance imaging and live ultrasound fusion. J Urol. 2011; 186(6):2214–2220. [PubMed: 22014798]
47. Smeenge M, de la Rosette JJ, Wijkstra H. Current status of transrectal ultrasound techniques in prostate cancer. Curr Opin Urol. 2012; 22(4):297–302. [PubMed: 22595778]

48. Anastasiadis AG, Lichy MP, Nagele U, Kuczyk MA, Merseburger AS, Hennenlotter J, Corvin S, Sievert KD, Claussen CD, Stenzl A, Schlemmer HP. MRI-guided biopsy of the prostate increases diagnostic performance in men with elevated or increasing PSA levels after previous negative TRUS biopsies. Eur Urol. 2006; 50(4):738–748. (discussion 748–739). [PubMed: 16630688]

49. Yakar D, Hambrock T, Hoeks C, Barentsz JO, Futterer JJ. Magnetic resonance-guided biopsy of the prostate: feasibility, technique, and clinical applications. Top Magn Reson Imaging TMRI. 2008; 19(6):291–295. [PubMed: 19512851]

50. Ukimura O, Hirahara N, Fujihara A, Yamada T, Iwata T, Kamoi K, Okihara K, Ito H, Nishimura T, Miki T. Technique for a hybrid system of real-time transrectal ultrasound with preoperative magnetic resonance imaging in the guidance of targeted prostate biopsy. Int J Urol Off J Jpn Urol Assoc. 2010; 17(10):890–893.

51. Ukimura O. Evolution of precise and multimodal MRI and TRUS in detection and management of early prostate cancer. Expert Rev Med Devices. 2010; 7(4):541–554. [PubMed: 20583890]

52. Siddiqui MM, Rais-Bahrami S, Turkbey B, George AK, Rothwax J, Shakir N, Okoro C, Raskolnikov D, Parnes HL, Linehan WM, Merino MJ, Simon RM, Choyke PL, Wood BJ, Pinto PA. Comparison of MR/ultrasound fusion-guided biopsy with ultrasound-guided biopsy for the diagnosis of prostate cancer. JAMA. 2015; 313(4):390–397. [PubMed: 25626035]

53. Marks L, Young S, Natarajan S. MRI-ultrasound fusion for guidance of targeted prostate biopsy. Curr Opin Urol. 2013; 23(1):43–50. [PubMed: 23138468]

54. Sonn GA, Natarajan S, Margolis DJ, MacAiran M, Lieu P, Huang J, Dorey FJ, Marks LS. Targeted biopsy in the detection of prostate cancer using an office based magnetic resonance ultrasound fusion device. J Urol. 2013; 189(1):86–91. [PubMed: 23158413]

55. Roehl KA, Antenor JA, Catalona WJ. Serial biopsy results in prostate cancer screening study. J Urol. 2002; 167(6)

56. Sonn GA, Chang E, Natarajan S, Margolis DJ, Macairan M, Lieu P, Huang J, Dorey FJ, Reiter RE, Marks LS. Value of targeted prostate biopsy using magnetic resonance-ultrasound fusion in men with prior negative biopsy and elevated prostate-specific antigen. Eur Urol. 2014; 65(4):809–815. [PubMed: 23523537]

57. Hu JC, Chang E, Natarajan S, Margolis DJ, Macairan M, Lieu P, Huang J, Sonn G, Dorey FJ, Marks LS. Targeted prostate biopsy in select men for active surveillance: do the Epstein criteria still apply? J Urol. 2014; 192(2):385–390. [PubMed: 24512956]

58. Le JD, Huang J, Marks LS. Targeted prostate biopsy: value of multiparametric magnetic resonance imaging in detection of localized cancer. Asian J Androl. 2014; 16(4):522–529. [PubMed: 24589455]

59. Sonn GA, Filson CP, Chang E, Natarajan S, Margolis DJ, Macairan M, Lieu P, Huang J, Dorey FJ, Reiter RE, Marks LS. Initial experience with electronic tracking of specific tumor sites in men undergoing active surveillance of prostate cancer. Urol Oncol. 2014; 32(7):952–957. [PubMed: 25027689]

60. Moore CM, Kasivisvanathan V, Eggener S, Emberton M, Futterer JJ, Gill IS, Grubb RL Iii, Hadaschik B, Klotz L, Margolis DJ, Marks LS, Melamed J, Oto A, Palmer SL, Pinto P, Puech P, Punwani S, Rosenkrantz AB, Schoots IG, Simon R, Taneja SS, Turkbey B, Ukimura O, van der Meulen J, Villers A, Watanabe Y. Standards of reporting for MRI-targeted biopsy studies (START) of the prostate: recommendations from an International Working Group. Eur Urol. 2013; 64(4): 544–552. [PubMed: 23537686]

61. Afshar-Oromieh A, Malcher A, Eder M, Eisenhut M, Linhart HG, Hadaschik BA, Holland-Letz T, Giesel FL, Kratochwil C, Haufe S, Haberkorn U, Zechmann CM. PET imaging with a [68Ga]gallium-labelled PSMA ligand for the diagnosis of prostate cancer: biodistribution in humans and first evaluation of tumour lesions. Eur J Nucl Med Mol Imaging. 2013; 40(4):486–495. [PubMed: 23179945]

62. Afshar-Oromieh A, Haberkorn U, Schlemmer HP, Fenchel M, Eder M, Eisenhut M, Hadaschik BA, Kopp-Schneider A, Rothke M. Comparison of PET/CT and PET/MRI hybrid systems using a 68Ga-labelled PSMA ligand for the diagnosis of recurrent prostate cancer: initial experience. Eur J Nucl Med Mol Imaging. 2014; 41(5):887–897. [PubMed: 24352789]

63. Eiber M, Maurer T, Souvatzoglou M, Beer AJ, Ruffani A, Haller B, Graner FP, Kubler H, Haberhorn U, Eisenhut M, Wester HJ, Gschwend JE, Schwaiger M. Evaluation of hybrid (6)(8)Ga-

PSMA ligand PET/CT in 248 patients with biochemical recurrence after radical prostatectomy. J Nucl Med Off Publ Soc Nucl Med. 2015; 56(5):668–674.

64. Eiber M, Weirich G, Holzapfel K, Souvatzoglou M, Haller B, Rauscher I, Beer AJ, Wester HJ, Gschwend J, Schwaiger M, Maurer T. Simultaneous (68)Ga-PSMA HBED-CC PET/MRI improves the localization of primary prostate cancer. Eur Urol. 2016; pii: S0302-2838(16)00011-7. doi: 10.1016/j.eururo.2015.12.053
65. Hara T, Kosaka N, Kishi H. PET imaging of prostate cancer using carbon-11-choline. J Nucl Med. 1998; 39(6):990–995. [PubMed: 9627331]
66. Carolan P, Hunt C, Murphy R, Johnson G, Peller P, Nathan M. Prostate cancer findings on FDG and C-11 choline PET/CT. Am J Roentgenol. 2012; 198:5. (abstract).
67. Schilling D, Schlemmer HP, Wagner PH, Bottcher P, Merseburger AS, Aschoff P, Bares R, Pfannenberg C, Ganswindt U, Corvin S, Stenzl A. Histological verification of ^{11}C-choline-positron emission/computed tomography-positive lymph nodes in patients with biochemical failure after treatment for localized prostate cancer. BJU Int. 2008; 102(4):446–451. [PubMed: 18410442]
68. Piert M, Park H, Khan A, Siddiqui J, Hussain H, Chenevert T, Wood D, Johnson T, Shah RB, Meyer C. Detection of aggressive primary prostate cancer with ^{11}C-choline PET/CT using multimodality fusion techniques. J Nucl Med Off Publ Soc Nucl Med. 2009; 50(10):1585–1593.
69. DeGrado TR, Baldwin SW, Wang S, Orr MD, Liao RP, Friedman HS, Reiman R, Price DT, Coleman RE. Synthesis and evaluation of (18)F-labeled choline analogs as oncologic PET tracers. J Nucl Med. 2001; 42(12):1805–1814. [PubMed: 11752077]
70. Soyka JD, Muster MA, Schmid DT, Seifert B, Schick U, Miralbell R, Jorcano S, Zaugg K, Seifert HH, Veit-Haibach P, Strobel K, Schaefer NG, Husarik DB, Hany TF. Clinical impact of F-18-choline PET/CT in patients with recurrent prostate cancer. Eur J Nucl Med Mol Imaging. 2012; 39(6):936–943. [PubMed: 22415598]
71. Kwee SA, DeGrado T. Prostate biopsy guided by ^{18}F-fluorocholine PET in men with persistently elevated PSA levels. Eur J Nucl Med Mol Imaging. 2008; 35(8):1567–1569. [PubMed: 18521597]
72. Oyama N, Miller TR, Dehdashti F, Siegel BA, Fischer KC, Michalski JM, Kibel AS, Andriole GL, Picus J, Welch MJ. ^{11}C-acetate PET imaging of prostate cancer: detection of recurrent disease at PSA relapse. J Nucl Med. 2003; 44(4):549–555. [PubMed: 12679398]
73. Mena E, Turkbey B, Mani H, Adler S, Valera VA, Bernardo M, Shah V, Pohida T, McKinney Y, Kwarteng G, Daar D, Lindenberg ML, Eclarinal P, Wade R, Linehan WM, Merino MJ, Pinto PA, Choyke PL, Kurdziel KA. ^{11}C-Acetate PET/CT in localized prostate cancer: a study with MRI and histopathologic correlation. J Nucl Med Off Publ Soc Nucl Med. 2012; 53(4):538–545.
74. Schiepers C, Hoh CK, Nuyts J, Seltzer M, Wu C, Huang SC, Dahlbom M. 1-^{11}C-acetate kinetics of prostate cancer. J Nucl Med. 2008; 49(2):206–215. [PubMed: 18199613]
75. Morris MJ, Scher HI. (11)C-acetate PET imaging in prostate cancer. Eur J Nucl Med Mol Imaging. 2007; 34(2):181–184. [PubMed: 17238014]
76. Lepin EJ, Leyton JV, Zhou Y, Olafsen T, Salazar FB, McCabe KE, Hahm S, Marks JD, Reiter RE, Wu AM. An affinity matured minibody for PET imaging of prostate stem cell antigen (PSCA)-expressing tumors. Eur J Nucl Med Mol Imaging. 2010; 37(8):1529–1538. [PubMed: 20354850]
77. Pillarsetty N, Punzalan B, Larson SM. 2-^{18}F-Fluoropro-pionic acid as a PET imaging agent for prostate cancer. J Nucl Med Off Publ Soc Nucl Med. 2009; 50(10):1709–1714.
78. Beattie BJ, Smith-Jones PM, Jhanwar YS, Schoder H, Schmidtlein CR, Morris MJ, Zanzonico P, Squire O, Meirelles GS, Finn R, Namavari M, Cai S, Scher HI, Larson SM, Humm JL. Pharmacokinetic assessment of the uptake of 16beta-^{18}F-fluoro-5alpha-dihydrotestosterone (FDHT) in prostate tumors as measured by PET. J Nucl Med Off Publ Soc Nucl Med. 2010; 51(2): 183–192.
79. Evans MJ, Smith-Jones PM, Wongvipat J, Navarro V, Kim S, Bander NH, Larson SM, Sawyers CL. Noninvasive measurement of androgen receptor signaling with a positron-emitting radiopharmaceutical that targets prostate-specific membrane antigen. Proc Natl Acad Sci USA. 2011; 108(23):9578–9582. [PubMed: 21606347]
80. Milowsky MI, Nanus DM, Kostakoglu L, Vallabhajosula S, Goldsmith SJ, Bander NH. Phase I trial of yttrium-90-labeled anti-prostate-specific membrane antigen monoclonal antibody J591 for

androgen-independent prostate cancer. J Clin Oncol. 2004; 22(13):2522–2531. [PubMed: 15173215]

81. Bander NH, Trabulsi EJ, Kostakoglu L, Yao D, Vallabhajosula S, Smith-Jones P, Joyce MA, Milowsky M, Nanus DM, Goldsmith SJ. Targeting metastatic prostate cancer with radiolabeled monoclonal antibody J591 to the extracellular domain of prostate specific membrane antigen. J Urol. 2003; 170(5):1717–1721. [PubMed: 14532761]
82. Shiiba M, Ishihara K, Kimura G, Kuwako T, Yoshihara N, Sato H, Kondo Y, Tsuchiya S, Kumita S. Evaluation of primary prostate cancer using C-11-methionine-PET/CT and F-18-FDG-PET/CT. Ann Nucl Med. 2012; 26(2):138–145. [PubMed: 22069194]
83. Nunez R, Macapinlac HA, Yeung HWD, Akhurst T, Cai SD, Osman I, Gonen M, Riedel E, Scher HI, Larson SM. Combined F-18-FDG and C-11-methionine PET scans in patients with newly progressive metastatic prostate cancer. J Nucl Med. 2002; 43(1):46–55. [PubMed: 11801702]
84. Lengyel Z, Toth G, Balkay L, Salah MA, Esik O, Sipos T, Tron L, Toth C. Detection of organ confined prostate cancer with ^{11}C-methionine PET. Eur J Nucl Med Mol Imaging. 2004; 31:S339.
85. Mease RC, Dusich CL, Foss CA, Ravert HT, Dannals RF, Seidel J, Prideaux A, Fox JJ, Sgouros G, Kozikowski AP, Pomper MG. 1,3-Dicarboxypropyl]carbamoyl]-4-F]fluorobenzyl–cysteine, [F]DCFBC: a new imaging probe for prostate cancer. Clin Cancer Res. 2008; 14(10):3036–3043. [PubMed: 18483369]
86. Cho SY, Gage KL, Mease RC, Senthamizhchelvan S, Holt DP, Jeffrey-Kwanisai A, Endres CJ, Dannals RF, Sgouros G, Lodge M, Eisenberger MA, Rodriguez R, Carducci MA, Rojas C, Slusher BS, Kozikowski AP, Pomper MG. Biodistribution, tumor detection, and radiation dosimetry of ^{18}F-DCFBC, a low-molecular-weight inhibitor of prostate-specific membrane antigen, in patients with metastatic prostate cancer. J Nucl Med Off Publ Soc Nucl Med. 2012; 53(12):1883–1891.
87. Rowe SP, Gage KL, Faraj SF, Macura KJ, Cornish TC, Gonzalez-Roibon N, Guner G, Munari E, Partin AW, Pavlovich CP, Han M, Carter HB, Bivalacqua TJ, Blackford A, Holt D, Dannals RF, Netto GJ, Lodge MA, Mease RC, Pomper MG, Cho SY. (1)(8)F-DCFBC PET/CT for PSMA-based detection and characterization of primary prostate cancer. J Nucl Med Off Publ Soc Nucl Med. 2015; 56(7):1003–1010.
88. Fei B, Wang H, Wu C, Chiu SM. Choline PET for monitoring early tumor response to photodynamic therapy. J Nucl Med Off Publ Soc Nucl Med. 2010; 51(1):130–138.
89. Schuster DM, Votaw JR, Nieh PT, Yu WP, Nye JA, Master V, Bowman FD, Issa MM, Goodman MM. Initial experience with the radiotracer anti-1-amino-3-F-18-fluorocyclobutane-1-carboxylic acid with PET/CT in prostate carcinoma. J Nucl Med. 2007; 48(1):56–63. [PubMed: 17204699]
90. Schuster DM, Taleghani PA, Nieh PT, Master VA, Amzat R, Savir-Baruch B, Halkar RK, Fox T, Osunkoya AO, Nye JA, Yu W, Fei BW, Wang Z, Chen Z, Goodman MM. Characterization of primary prostate carcinoma by anti-1-amino-2-[^{18}F]-fluorocyclobutane-1-carboxylic acid (anti-3-[^{18}F] FACBC) uptake. Am J Nucl Med Mol Imaging. 2013; 3(1):85–96. [PubMed: 23342303]
91. Oka S, Hattori R, Kurosaki F, Toyama M, Williams LA, Yu W, Votaw JR, Yoshida Y, Goodman MM, Ito O. A preliminary study of anti-1-amino-3-^{18}F-fluorocyclobutyl-1-carboxylic acid for the detection of prostate cancer. JNuclMed. 2007; 48(1):46–55.
92. Schuster DM, Nieh PT, Jani AB, Amzat R, Bowman FD, Halkar RK, Master VA, Nye JA, Odewole OA, Osunkoya AO, Savir-Baruch B, Alaei-Taleghani P, Goodman MM. Anti-3-[(18)F]FACBC positron emission tomography-computerized tomography and (111)In-capromab pendetide single photon emission computerized tomography-computerized tomography for recurrent prostate carcinoma: results of a prospective clinical trial. J Urol. 2014; 191(5):1446–1453. [PubMed: 24144687]
93. Schuster DM, Taleghani PA, Nieh PT, Master VA, Amzat R, Savir-Baruch B, Halkar RK, Fox T, Osunkoya AO, Moreno CS, Nye JA, Yu W, Fei B, Wang Z, Chen Z, Goodman MM. Characterization of primary prostate carcinoma by anti-1-amino-2-[(18)F]-fluorocyclobutane-1-carboxylic acid (anti-3-[(18)F] FACBC) uptake. Am J Nucl Med Mol Imaging. 2013; 3(1):85–96. [PubMed: 23342303]
94. Turkbey B, Mena E, Shih J, Pinto PA, Merino MJ, Lindenberg ML, Bernardo M, McKinney YL, Adler S, Owenius R, Choyke PL, Kurdziel KA. Localized prostate cancer detection with ^{18}F FACBC PET/CT: comparison with MR imaging and histopathologic analysis. Radiology. 2014; 270(3):849–856. [PubMed: 24475804]

95. Fei, B., Master, V., Nieh, P., Akbari, H., Yang, X., Fenster, A., Schuster, D. A PET/CT directed, 3D ultrasound-guided biopsy system for prostate cancer. In: Workshop on Prostate Cancer Imaging. The Annual Meeting of the Society of Medical Imaging Computing and Image Assisted Interventions (MIC-CAI), Lecture Notes in Computer Science, 2011. Workshop on Prostate Cancer Imaging at the Medical Imaging Computing and Image Assisted Interventions Meeting (MICCAI 2011)—Lecture Notes in Computer Science; 2011. p. 100-108.

96. Fei B, Nieh PT, Schuster DM, Master VA. PET-directed, 3D Ultrasound-guided prostate biopsy. Diagn Imaging Eur. 2013; 29(1):12–15. [PubMed: 25392702]

97. Fei, B., Schuster, DM., Master, V., Akbari, H., Fenster, A., Nieh, P. A molecular image-directed, 3D ultrasound-guided biopsy system for the prostate. Proc SPIE. Int Soc Opt Eng; 2012. pii: 831613

98. Akbari H, Fei BW. 3D ultrasound image segmentation using wavelet support vector machines. Med Phys. 2012; 39(6):2972–2984. [PubMed: 22755682]

99. Qiu W, Yuan J, Ukwatta E, Sun Y, Rajchl M, Fenster A. Dual optimization based prostate zonal segmentation in 3D MR images. Med Image Anal. 2014; 18(4):660–673. [PubMed: 24721776]

100. Mahapatra D, Buhmann JM. Prostate MRI segmentation using learned semantic knowledge and graph cuts. Biomed Eng IEEE Trans. 2014; 61(3):756–764.

101. Litjens G, Debats O, Barentsz J, Karssemeijer N, Huisman H. Computer-aided detection of prostate cancer in MRI. IEEE Trans Med Imaging. 2014; 33(5):1083–1092. [PubMed: 24770913]

102. Liao S, Gao Y, Oto A, Shen D. Representation learning: a unified deep learning framework for automatic prostate MR segmentation. Med Image Comput Comput Assist Interv MIC-CAI Int Conf Med Image Comput Comput Assist Interv. 2013; 16(Pt 2):254–261.

103. Toth R, Madabhushi A. Multifeature landmark-free active appearance models: application to prostate MRI segmentation. IEEE Trans Med Imaging. 2012; 31(8):1638–1650. [PubMed: 22665505]

104. Litjens G, Debats O, van de Ven W, Karssemeijer N, Huisman H. A pattern recognition approach to zonal segmentation of the prostate on MRI. Med Image Comput Comput Assist Interv MICCAI Int Conf Med Image Comput Comput Assist Interv. 2012; 15(Pt 2):413–420.

105. Qiu W, Yuan J, Ukwatta E, Sun Y, Rajchl M, Fenster A. Prostate segmentation: an efficient convex optimization approach with axial symmetry using 3-D TRUS and MR images. IEEE Trans Med Imaging. 2014; 33(4):947–960. [PubMed: 24710163]

106. Yang M, Li X, Turkbey B, Choyke PL, Yan P. Prostate segmentation in MR images using discriminant boundary features. Biomed Eng IEEE Trans. 2013; 60(2):479–488.

107. Zwiggelaar, R., Zhu, Y., Williams, S. Pattern recognition and image analysis. Springer; New York: 2003. Semi-automatic segmentation of the prostate; p. 1108-1116.

108. Flores-Tapia, D., Thomas, G., Venugopa, N., McCurdy, B., Pistorius, S. Semi automatic MRI prostate segmentation based on wavelet multiscale products. Engineering in medicine and biology society EMBS; 30th Annual International Conference of the IEEE, 2008. IEEE; 2008. p. 3020-3023.

109. Samiee, M., Thomas, G., Fazel-Rezai, R. Semi-automatic prostate segmentation of MR images based on flow orientation. Signal processing and information technology, 2006 IEEE International Symposium on; 2006; IEEE; p. 203-207.

110. Cootes, TF., Hill, A., Taylor, CJ., Haslam, J. Information processing in medical imaging. Springer; New York: 1993. The use of active shape models for locating structures in medical images; p. 33-47.

111. Zhu Y, Williams S, Zwiggelaar R. A hybrid ASM approach for sparse volumetric data segmentation. Pattern recognition and image analysis. 2007; 17(2):252–258.

112. Kass M, Witkin A, Terzopoulos D. Snakes: active contour models. Int J Comput Vis. 1988; 1(4): 321–331.

113. Chan TF, Vese LA. Active contours without edges. IEEE Trans Image Process. 2001; 10(2):266–277. [PubMed: 18249617]

114. Mumford D, Shah J. Optimal approximations by piecewise smooth functions and associated variational problems. Commun Pure Appl Math. 1989; 42(5):577–685.

115. Ghose S, Oliver A, Marti R, Llado X, Vilanova JC, Freixenet J, Mitra J, Sidibe D, Meriaudeau F. A survey of prostate segmentation methodologies in ultrasound, magnetic resonance and computed tomography images. Comput Methods Programs Biomed. 2012; 108(1):262–287. [PubMed: 22739209]
116. Klein S, van der Heide UA, Lips IM, van Vulpen M, Staring M, Pluim JPW. Automatic segmentation of the prostate in 3D MR images by atlas matching using localized mutual information. Med Phys. 2008; 35(4):1407–1417. [PubMed: 18491536]
117. Egger J. PCG-cut: graph driven segmentation of the prostate central gland. PLoS One. 2013; 8(10):6.
118. Tian Z, Liu L, Zhang Z, Fei B. Superpixel-based Segmentation for 3D prostate MR images. IEEE Trans Med Imaging. 2016; 35(3):791–801. [PubMed: 26540678]
119. Tian Z, Liu L, Fei B. A supervoxel-based segmentation for prostate MR images. Proc SPIE. 2015; 9731:941318.
120. Fei, BW., Schuster, DM., Master, VA., Nieh, PT. Incorporating PET/CT images into 3D ultrasound-guided biopsy of the prostate. Med Phys; The Annual Meeting of the American Association of Physics in Medicine (AAPM); Charlotte, NC. 2012; 2012. p. 3888
121. Fei, BW., Master, V., Nieh, P., Akbari, H., Yang, XF., Fenster, A., Schuster, D. A PET/CT directed, 3D ultrasound-guided biopsy system for prostate cancer. In: Madabhushi, A.Dowling, J.Huisman, H., Barratt, D., editors. Prostate cancer imaging: image analysis and image-guided interventions, vol. 6963. Lecture Notes in Computer Science. Springer; Piscataway, NJ: 2011. p. 100-108.
122. Oliveira FP, Tavares JMR. Medical image registration: a review. Comput Methods Biomech Biomed Eng. 2014; 17(2):73–93.
123. Neto JA, Parente DB. Multiparametric magnetic resonance imaging of the prostate. Magn Reson Imaging Clin N Am. 2013; 21:409–426. [PubMed: 23642560]
124. Mease RC, Foss CA, Pomper MG. PET imaging in prostate cancer: focus on prostate-specificmembrane antigen. Curr Top Med Chem. 2013; 13:951–962. [PubMed: 23590171]
125. The diagnostic value of PET/CT imaging with the. (68)Ga-labelled PSMA ligand HBED-CC in the diagnosis of recurrent prostate cancer. Eur J Nucl Med Mol Imaging. 2015; 42(2):197–209. [PubMed: 25411132]
126. Herlemann A, Wenter V, Kretschmer A, Thierfelder KM, Bartenstein P, Faber C, Gildehaus FJ, Stief CG, Gratzke C, Fendler WP. (68)Ga-PSMA positron emission tomography/computed tomography provides accurate staging of lymph node regions prior to lymph node dissection in patients with prostate cancer. Eur Urol. 2016 pii: S0302-2838(16)00009-9.
127. Maurer T, Gschwend JE, Rauscher I, et al. Diagnostic efficacy of 68gallium-PSMA positron emission tomography compared to conventional imaging for lymph node staging of 130 consecutive patients with intermediate to high risk prostate cancer. J Urol. 2016; 195:1436–1443. [PubMed: 26682756]
128. Pomper MG, Musachio JL, Zhang J, et al. ^{11}C-MCG: synthesis, uptake selectivity, and primate PET of a probe for glutamate carboxypeptidase II (NAALADase). Mol Imaging. 2002; 1:96–101. [PubMed: 12920850]
129. Cho SY, Gage KL, Mease RC, et al. Biodistribution, tumor detection, and radiation dosimetry of [r]18[/r]F-DCFBC, a low-molecular-weight inhibitor of prostate-specific membrane antigen, in patients with metastatic prostate cancer. J Nucl Med. 2012; 53:1883–1891. [PubMed: 23203246]
130. Muller, et al. Multiparametric magnetic resonance imaging-transrectal ultrasound fusion–assisted biopsy for the diagnosis of local recurrence after radical prostatectomy. Urol Oncol. 2015; 33(10):425, e1–6.
131. Sankineni S, et al. Posterior subcapsular prostate cancer-identification with mpMRI and MRI TRUS fusion-guided biopsy. Abdom Imaging. 2015; 40(7):2557–2565. [PubMed: 25916869]
132. Walton Diaz A, et al. Can magnetic resonance-ultrasound fusion biopsy improve cancer detection in enlarged prostates? J Urol. 2013; 190(6):2020–2025. [PubMed: 23792130]
133. Le JD, et al. Magnetic resonance imaging-ultrasound fusion biopsy for prediction of final prostate pathology. J Urol. 2014; 192(5):1367–1373. [PubMed: 24793118]

134. Filson CP, et al. Prostate cancer detection with magnetic resonance-ultrasound fusion biopsy: the role of systematic and targeted biopsies. Cancer. 2016; 122(6):884–892. [PubMed: 26749141]

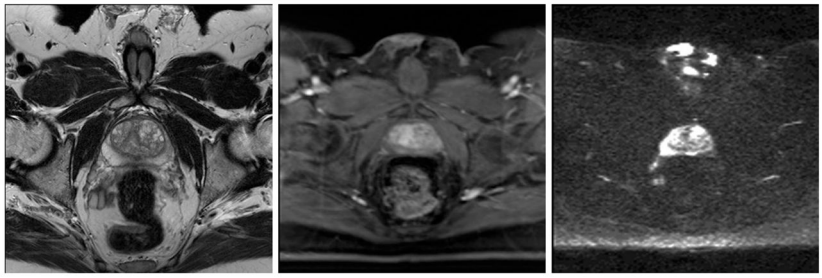

Fig. 1.

Multiparametric MRI of the prostate: T2-weighted MRI (*left*), DCE-MRI (*middle*), and diffusion-weighted MRI (*right*) of the same patient

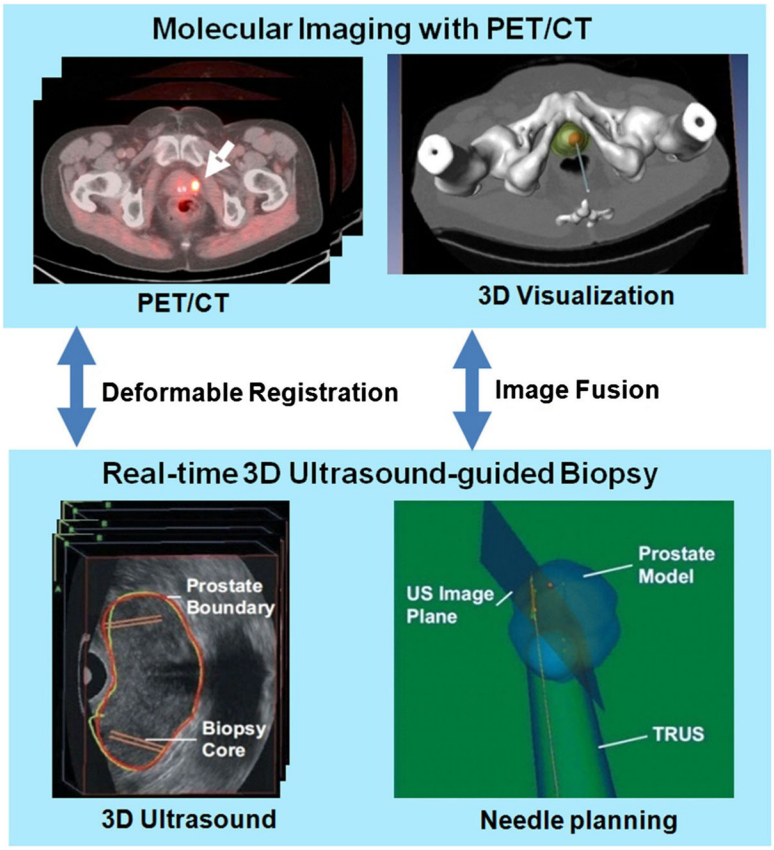

Fig. 2.

PET/ultrasound fusion targeted biopsy. *Top* the PET/CT images with fluciclovine were acquired from a human subject. PET/CT images show a focal lesion within the prostate (*white arrow*). The 3D visualization of the pelvis and the prostate were used to aid the planning of the biopsy to a suspicious tumor target. *Bottom* during biopsy, a mechanically assisted navigation device, was used to acquire 3D TRUS images from patients. The prostate boundaries on TRUS images were segmented and were used to generate a 3D model of the prostate. The 3D prostate model and real-time TRUS images are used to guide the biopsy in patients [96]

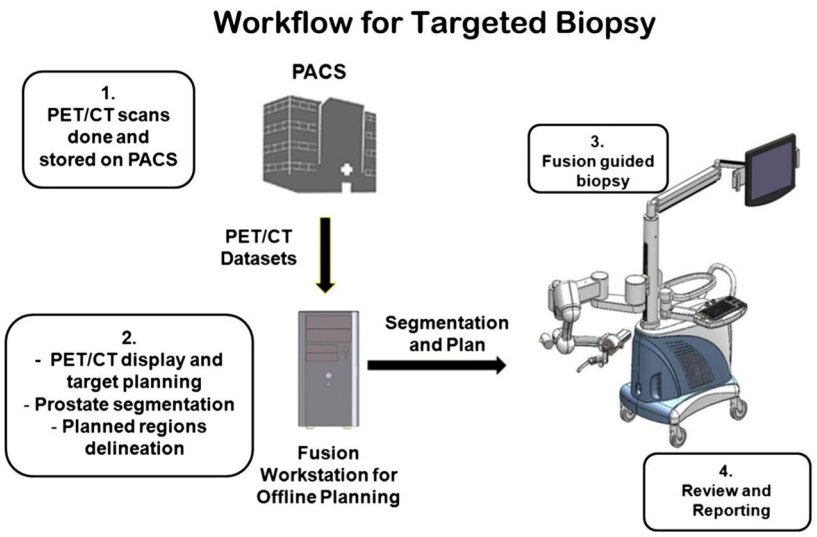

Fig. 3.
Clinical workflow for the PET/ultrasound fusion targeted biopsy

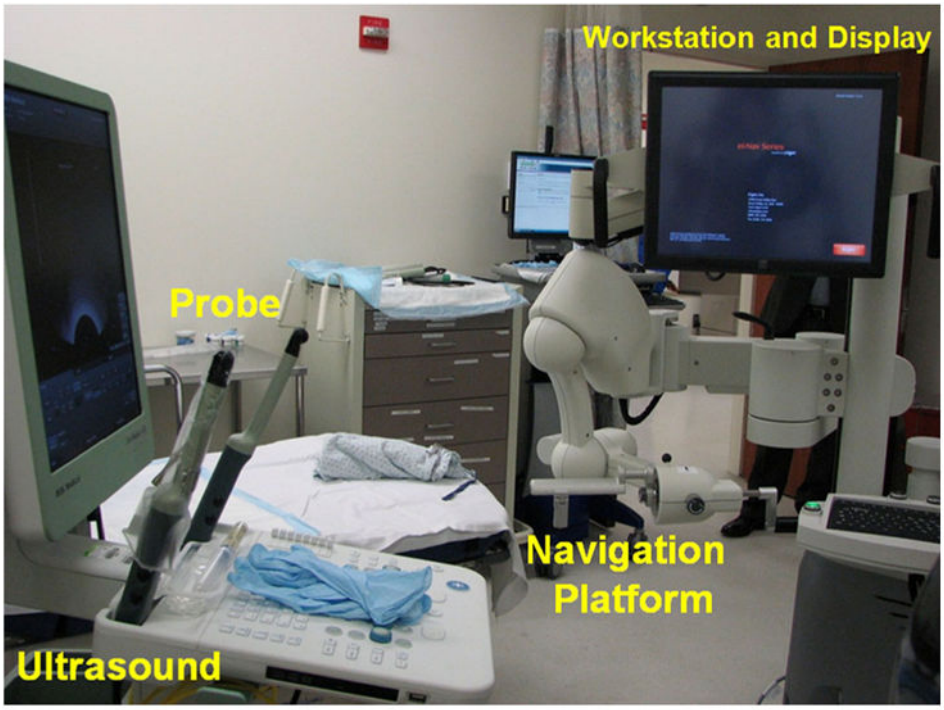

Fig. 4.

Setup for the molecular image-directed, 3D ultrasound-guided biopsy system that includes a commercial ultrasound scanner and an end firing probe from B&K Medical, the Artemis system, and a workstation for image fusion

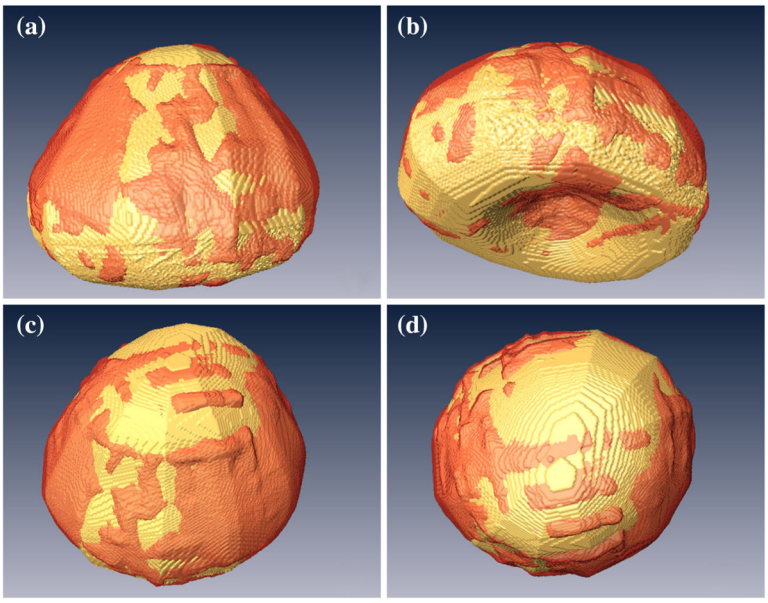

Fig. 5.

3D visualization of the automatically segmented prostate (*red*) as compared with the manual segmentation gold standard (*gold color*) in *four different views* (**a**–**d**) of the same human prostate Reprint from Akbari et al. [98]

Table 1

Selected studies on MR/TURS fusion targeted biopsy by the NCI and UCLA groups

Study	Patient demographics			MR				Fusion platform	Underwent 12-core systematic biopsy	Target biopsy		
	Sample size (*n*)	Mean/Median age (year)	Median PSA (ng/ml)	Median prostate volume (cc)	MR scanner	ER coil	Average lesions per patient			Cores per patient	Cores per lesion	Overall cancer detection
Pinto et al. 2011 [38]	101	63 (41–82)	5.8 (0.2–103)	–	3.0T, Achieva, Philips	Yes	2.6 (1–7)	UroNav	Yes	5.8	2.2 (1–8)	27.9%, 66.7%, 89.5%^
Vourganti et al. 2012 [40]	195	62 (37–80)	9.13 (0.3–103)	56 (16–187)	3.0T, Achieva, Philips	Yes	2 (1–7)	UroNav	Yes	–	–	15.22%, 38.14%, 67.14%^
Siddiqui et al. 2015 [52]	1003	62	6.7 (4.4–10.7)	49 (36–71)	3.0T, Achieva, Philips	Yes	2.7	UroNav	Yes	5.3	–	46.0% (461/1003)
Sonn et al. 2013 [54]	171	65	4.9	48	3.0T, Somatom, Siemens	No	1.6 (0–4)	Artemis	Yes	13.4	2.2 (1–6)	48%, 56%, 94% *
Sonn et al. 2014 [56]	105	65 (59–70)	7.5 (5.0–11.2)	58 (39–82)	3.0T, Somatom, Siemens	No	1.3 (1–3)	Artemis	Yes	15.9	4.2 (1–9)	4%, 21%, 75% *
Hu et al. 2014 [57]	113	63 (58–68)	4.2 (2.6–6.3)	46.8 (36.1–64.5)	3.0T, Somatom, Siemens	No	–	Artemis	Yes	4	–	77%
Sonn et al. 2014 [59]	53	64 (59–69)	4.3 (2.2–6.4)	48 (36–60)	3.0T, Somatom, Siemens	No	–	Artemis	Yes	–	–	39%
Muller et al. 2015 [130]	10	63 (56–68)	–	–	3.0T, Achieva, Philips	Yes	1.6	UroNav	No	–	–	80% (8/10)
Sankineni et al. 2015 [131]	33	63 (52–76)	6.1 (1.22–65.2)	53 (12–125)	3.0T, Achieva, Philips	Yes	–	UroNav	Yes	–	–	72.7% (24/33)
Walton et al. 2013 [132]	649	62	6.65	58.7	3.0T, Achieva, Philips	Yes	–	UroNav	Yes	–	–	55% (357/649)
Le et al. 2014 [133]	54	62	6.2 (5.0–10.9)	–	3.0T, Somatom, Siemens	No	1.9	Artemis	Yes	5.9 (4–8)	–	5.5%, 69%, 75% *
Filson et al. 2016 [134]	1042	65.7 (59.3–70.2) +	7.6 (5.0–11.5) +	57.7 (39.8–83.5) +–	3.0T, Somatom, Siemens	No	1.5	Artemis	Yes	–	–	16%, 33%, 69% *

ER endorectal, – Not available

* For regions of interest (ROIs) on MRI with Grade 3, 4, and 5, respectively

^ For patients with low, moderate, and high suspicion, respectively

\+ The group of prior negative biopsy (N=324)